ACS OMEGA

http://pubs.acs.org/journal/acsodf

Article

Computational Search for Better Thermoelectric Performance in Nickel-Based Half-Heusler Compounds

Xiaorui Chen, Xin Zhang, Jianzhi Gao, Qing Li, Zhibin Shao,* Haiping Lin,* and Minghu Pan*

Cite This: *ACS Omega* 2021, 6, 18269−18280

Read Online

ACCESS | Metrics & More | Article Recommendations

ABSTRACT: Half-Heusler alloys have recently received extensive attention because of their promising thermoelectric (TE) properties and great potential for applications requiring efficient thermoelectricity. Although the conversion efficiency of these materials can be greatly improved by doping, it is still far away from the real-life applications. Therefore, search for better parent TE compounds is deemed urgent. Using a high-throughput search method based on first-principles calculations in newly proposed 378 half-Heusler alloys, we identify nine nickel-based half-Heusler semiconductors as candidates and systematically study their mechanical, electronic, and transport properties. Their mechanical and dynamical stabilities are verified based on the calculated elastic constants and phonon spectra. The electronic structure calculations indicate the existence of direct energy gaps in the NiVZ (Z = Al, Ga, and In) and indirect energy gaps in the NiTiZ (Z = Si, Ge, and Sn) and NiScZ (Z = P, As, and Sb) compounds. Among them, NiVAl, NiVGa, and NiVIn exhibit a sharp slope of density of states near the Fermi level, which is predicted to be essential for a high TE performance. Further investigation on carrier concentration and temperature dependence of TE properties shows the high power factors of NiVAl, NiVGa, and NiVIn, which are responsible for their high figure of merit values. The highest maximum power factor of 5.152 mW m^{-1} K^{-2} and figure of merit of 0.309 are predicted for pristine half-Heusler NiVIn, which are larger than the values of some known pristine and doped half-Heusler TE materials. Our work opens up new avenues for rationally searching better TE materials among half-Heusler alloys for applications in fields requiring efficient thermoelectricity.

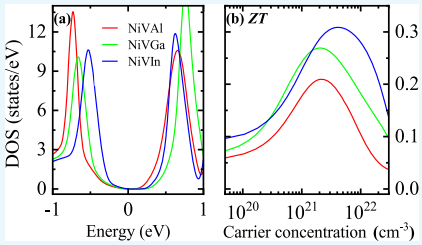

INTRODUCTION

Thermoelectric (TE) materials, which can convert heat to electricity and vice versa, have been extensively studied for their promising applications in both electric power generation and cooling during the past decades. The conversion efficiency of TE materials is characterized by the dimensionless figure of merit $ZT = S^2\sigma T/(\kappa_e + \kappa_l)$.[1] Here, S, σ, and T are the Seebeck coefficient, electrical conductivity, and absolute temperature, respectively. κ_e (κ_l) is the thermal conductivity contributed by electrons (phonons). An ideal TE material should have a large power factor defined as PF = $S^2\sigma$, a low thermal conductivity ($\kappa = \kappa_e + \kappa_l$), and hence a high ZT. Unfortunately, the Seebeck coefficient and electrical conductivity are commonly anticorrelated and a large electrical conductivity corresponds to a large electronic thermal conductivity, thus causing the reduction of ZT. Due to the interdependency of these transport coefficients (S, σ, and κ_e), it is a great challenge to enhance the value of ZT. The figure of merit for a given TE material is proportional to $(m^*)^{3/2}\mu$, in which m^* and μ are, respectively, the effective mass and carrier mobility. The behavior of m^* and μ can be characterized by $\mu = e\tau/m^*$. As a result, the power factor can be optimized by enhancing m^* with slightly reducing μ. A sharp slope of density of states (DOS) near the band gap always gives a large effective mass and therefore a high Seebeck coefficient. Therefore, a strategy for achieving a higher ZT value is to search for TE materials with a sharp slope of DOS near the band gap.

Ternary half-Heusler alloys, with a valence electron count of 18, have been recently studied as promising candidates for TE materials due to the narrow band gap, large Seebeck coefficient, moderate electrical conductivity, good mechanical properties, and thermal stability.[2] On the other hand, ternary half-Heusler alloys can be easily synthesized into 100% dense samples,[3] and their TE efficiency can be further improved by isoelectronic alloying.[4] Until now, the most studied half-Heusler TE compounds are the MNiSn- and MCoSb-related (M = Ti, Zr, and Hf) compounds.[5−7] Good pristine half-Heusler compounds such as TiCoSb and ZrNiSn hold large ZT values in the range of 0.015−0.3.[8,9] In recent years, considerable effort has be made to enhance the TE efficiency of the half-Heusler semiconductors by isoelectronic doping. The ZT in HfNiSn is enhanced up to 1.0 by doping Zr and Sb for the substitution of Hf and Sn, respectively.[10] In n-type

Received: April 23, 2021
Accepted: July 1, 2021
Published: July 12, 2021

ACS Publications

© 2021 The Authors. Published by American Chemical Society

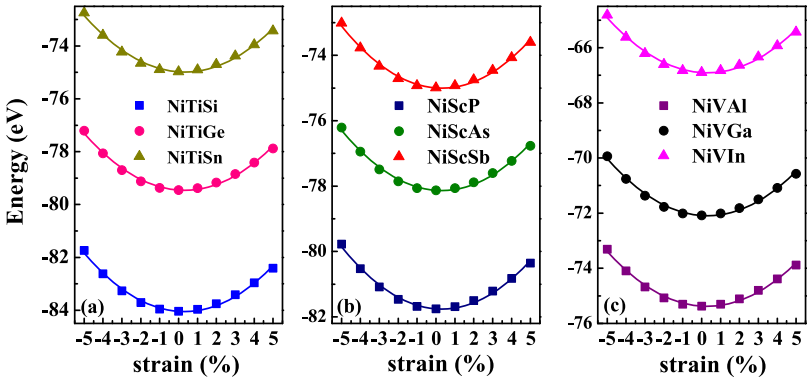

Figure 1. Total energy as a function of lattice strain that varies in the range of −5 to 5% for NiTiZ (Z = Si, Ge, and Sn) (a), NiScZ (Z = P, As, and Sb) (b), and NiVZ (Z = Al, Ga, and In) (c). The dots and solid lines are, respectively, the calculated results and fitted data.

Table 1. Calculated Lattice Constants (a) (in Å), Distance from the Convex Hull for the $C1_b$ Phase ($\Delta E_{HD}^{C1_b}$) (in eV/atom), Elastic Constants (C_{ij}), Bulk Modulus (B), Shear Modulus (G), Young's Modulus (E) (in GPa), Pugh's Ratio (B/G), and Poisson's Ratio (υ) for NiYZ (Y = Ti, Sc, and V; Z = Si, Ge, Sn, P, As, Sb, Al, Ga, and In) Alloys, Together with the Available Theoretical Results

	NiTiSi	NiTiGe	NiTiSn	NiScP	NiScAs	NiScSb	NiVAl	NiVGa	NiVIn
a	5.572	5.664	5.944	5.692	5.846	6.124	5.582	5.564	5.852
	5.56[a]	5.65[a]	5.93[a]	5.67[a]	5.82[a]	6.10[a]	5.57[a]	5.55[a]	5.84[a]
	5.58[b]	5.67[b]	5.96[b]	5.69[b]	5.85[b]	6.13[b]	5.60[b]	5.58[b]	5.86[b]
			5.94[c]						
			5.89[d]			6.06[d]			
$\Delta E_{HD}^{C1_b}$	0.084[a]	0[a]	0[a]	0.169[a]	0.035[a]	0[a]	0.230[a]	0.108[a]	0.280[a]
C_{11}	268.289	243.887	220.794	211.137	191.568	191.435	249.538	239.206	210.753
			196.41[e]						
C_{12}	113.684	108.598	82.408	83.046	71.309	55.190	109.286	120.005	102.524
			82.16[e]						
C_{44}	93.818	86.239	61.173	71.472	71.052	64.754	68.578	70.506	27.561
			62[d]			66[d]			
			60.61						
B	165.219	153.694	128.537	125.743	111.395	100.605	156.036	159.739	138.600
			120.24[e]						
G	86.822	78.249	64.264	68.403	66.461	66.081	69.193	65.698	34.292
			59.19[e]						
B/G	1.903	1.964	2.000	1.838	1.676	1.522	2.255	2.423	3.825
			2.03[e]						
E	221.641	200.688	165.252	173.709	166.309	162.635	180.848	173.848	99.997
			152.54[e]						
υ	0.276	0.282	0.286	0.270	0.251	0.231	0.307	0.319	0.380
			0.29[e]						

[a]Reference 17. [b]Reference 22. [c]Reference 23. [d]Reference 24. [e]Reference 25.

$Hf_{0.6}Zr_{0.4}NiSn_{0.995}Sb_{0.005}$ alloys, an even higher ZT value of 1.2 has been obtained at 900 K.[11] Studies on doped-(Ti, Zr, or Hf)NiSn compounds show that the doping of Sb instead of Sn remarkably reduces the electrical resistivity and hence enhances ZT to 1.5 at 700 K.[12] Other reliable half-Heusler TE materials are from the family of FeMSb-related (M = Nb and Ti) compounds with large ZT values of 1.1−1.5.[13−16] However, these high maximum values of ZT are all achieved by experimentally mixing M elements with each other or substituting Sn for Sb. The conversion efficiency of these doped half-Heusler TE materials is still far away from the real application. The search for better parent compounds becomes more essential for higher ZT values and conversion efficiency of TE materials.

New 378 types of half-Heusler alloys have been proposed and have great potential for applications in various areas.[17] Among them, the nine nickel-based half-Heusler semiconductors NiYZ (Y = Ti, Sc, and V; Z = Si, Ge, Sn, P, As, Sb, Al, Ga, and In) have the same crystalline structure as compounds such as TiCoSb and ZrNiSn, whose pristine compounds have large ZT values, as mentioned above. The nickel element is of low-cost and earth-abundant, which is economic to realize large-scale industrial applications in TE matrices. Two works[18,19] have predicted the TE properties of NiTiZ (Z = Si, Ge, and Sn) by treating the carrier relaxation time as a constant. However, the validity of TE properties based on the constant carrier relaxation time approximation is questionable.[20] In our study, the carrier relaxation time is determined by adopting the deformation potential (DP)

https://doi.org/10.1021/acsomega.1c02172
ACS Omega 2021, 6, 18269−18280

theory, which is proved to be able to produce accurate results of electrical transport properties, compared to experiments, for FeNbSb-based TE materials.[21] Here, we perform a detailed study on mechanical, electronic, and TE properties of NiYZ (Y = Ti, Sc, and V; Z = Si, Ge, Sn, P, As, Sb, Al, Ga, and In) groups. Among them, we find a sharp slope of DOS near the Fermi level in nickel-based semiconductors, which can serve as a hint for the search of promising TE materials.

■ RESULTS AND DISCUSSION

Structural Stability. A half-Heusler alloy with a chemical formula of *XYZ* crystallizes in the cubic MgAgAs-type $C1_b$ structure with the space group of $F\bar{4}3m$. In the Wyckoff coordinate, X atoms are located at 4c (0.25, 0.25, 0.25). Y and Z atoms occupy 4b (0.5, 0.5, 0.5) and 4a (0, 0, 0), respectively. In our study, X is Ni, Y is one of Ti, Sc, or V, and Z is one of Si (Ge, Sn), P (As, Sb), or Al (Ga, In). As a result, there are nine half-Heusler compounds with 18 valence electrons in this study. We first carry out the structural optimization by calculating the total energy when the lattice strain varies in the range of −5 to 5%, as shown in Figure 1. The obtained equilibrium lattice constants for these nine half-Heusler compounds with other theoretical results[17,22−25] are listed in Table 1. The discrepancy between our calculated results and available data is inappreciable, indicating the reliability of the method used in this work. Based on the corresponding total energy with lattice strain, the obtained elastic constants (*C*) for nine half-Heusler compounds are listed in Table 2. At the same time, the band-edge energies for electrons and holes as a function of the lattice strain are plotted in Figure 2. They show good linear dependence. It can be clearly seen from Figure 2 that the differences in the energy of the valence band maximum (VBM) and conduction band minimum (CBM) for NiTiSi and NiTiGe shrink as the lattice strain changes from −5 to 5%. As a result, this induces a large difference of DP constant for electrons and holes in case of NiTiSi and NiTiGe. However, the energy of the VBM and CBM for other seven half-Heusler alloys in this study shows a trend similar to the lattice strain, thus resulting in the nearly same DP constant for electrons and holes as listed in Table 2.

Table 2. Calculated Elastic Constant (*C*), DP Constant (E_1), Band Effective Mass (m_b^*), and Obtained Relaxation Time (τ) at Room Temperature

system	carrier type	C (GPa)	E_1 (eV)	m_b^* (m_e)	τ (fs)
NiTiSi	electrons	156.566	26.456	1.1991	2.781
	holes	156.566	23.474	3.914	1.281
NiTiGe	electrons	144.410	23.988	2.019	3.055
	holes	144.410	21.756	3.165	1.892
NiTiSn	electrons	123.115	24.831	1.549	3.618
	holes	123.115	23.835	3.029	1.435
NiScP	electrons	125.850	28.616	7.477	0.263
	holes	125.850	28.523	0.668	9.905
NiScAs	electrons	112.640	29.035	18.083	0.061
	holes	112.640	29.373	0.614	9.476
NiScSb	electrons	100.903	25.729	2.821	1.124
	holes	100.903	25.693	0.645	10.299
NiVAl	electrons	140.833	27.942	1.635	3.012
	holes	140.833	28.348	0.445	20.613
NiVGa	electrons	146.210	24.444	1.521	4.555
	holes	146.210	24.004	0.665	16.356
NiVIn	electrons	121.553	27.299	1.693	2.585
	holes	121.553	26.855	0.473	18.072

We then analyze mechanical properties of nine half-Heusler compounds. They all belong to cubic crystals and there are only three independent elastic stiffness coefficients (C_{11}, C_{12}, and C_{44}),[26] summarized in Table 1. For a cubic crystal at $P = 0$ GPa, the mechanical stability criterion is in the order of $C_{11} + 2C_{12} > 0$, $C_{44} > 0$, and $C_{11} - C_{12} > 0$.[27,28] All the studied crystals are mechanically stable. In accordance with the Voigt−Reuss−Hill approximation, other elastic properties such as bulk modulus (*B*), shear modulus (*G*), Pugh's ratio (*B*/*G*), Young's modulus (*E*), and Poisson's ratio (υ) are calculated and listed in Table 1. The relatively high bulk modulus of all the listed compounds shows the difficulty of compressing these materials. The shear modulus is known to provide more accurate information about hardness than the bulk modulus. Apparently, NiTiSi has the largest shear modulus of 86.822 GPa among the nine half-Heusler compounds, suggesting its strong resistance to shape change. The ratio of bulk to shear modulus (*B*/*G*) is an important parameter to describe the ductile or brittle behavior of a material with the critical value of 1.75.[29] The value of *B*/*G* lower than (or higher than) 1.75 indicates the brittleness (or ductility). According to Table 1, NiScAs and NiScSb are brittle, while the other seven half-Heusler alloys exhibit ductile behavior. As is well known, Young's modulus (*E*) defined as the ratio between stress and strain offers a correlation with stiffness. A stiffer material has a larger value of *E*. As shown in Table 1, NiTiSi has the largest *E* (221.641 GPa) and is much stiffer than other materials in this study. According to Frantsevich's rule,[30] Poisson's ratio is used to quantify the ductile and brittle nature of a material. The critical value is 0.26. For ductile materials, Poisson's ratio is larger than 0.26; otherwise, the materials behave in a brittle manner. It can be observed in Table 1 that the value of Poisson's ratio is smaller than 0.26 for NiScAs and NiScSb, indicating the brittle nature of NiScAs and NiScSb. The other seven half-Heusler alloys in this study behave in a ductile manner. This agrees well with the estimation from Pugh's ratio.

Analysis of phonon dispersion curves provides a reliable criterion for the dynamical stability. When the calculated dispersions of phonon modes have positive square of frequency throughout the Brillouin zone, the crystal structures are confirmed to be dynamically stable. Otherwise, the imaginary frequency indicates the dynamically unstable structures. With the purpose of checking the dynamical stability of the NiYZ (Y = Ti, Sc, and V; Z = Si, Ge, Sn, P, As, Sb, Al, Ga, and In) crystallized in the half-Heusler structure, Figure 3 presents the calculated dispersion of phonon modes of NiYZ (Y = Ti, Sc, and V; Z = Si, Ge, Sn, P, As, Sb, Al, Ga, and In) in the half-Heusler structure. It points out that our phonon band structure of NiTiSn is nearly the same as the result obtained in another theoretical work conducted on NiTiSn,[23] indicating the reasonability of the computational method used in this study. The calculated phonon dispersions for the nine systems are all composed of three acoustic modes and six optical ones because there are three atoms in the primitive cell of the NiYZ compounds. There are no imaginary frequencies in the phonon dispersion curves in the whole Brillouin zone. These results indicate that the half-Heusler NiYZ (Y = Ti, Sc, and V; Z = Si, Ge, Sn, P, As, Sb, Al, Ga, and In) are dynamically stable. As the errors in the density functional theory (DFT) formation energy cannot be directly used as the error bars when considering the stability and metastability of a compound, the

https://doi.org/10.1021/acsomega.1c02172
ACS Omega 2021, 6, 18269−18280

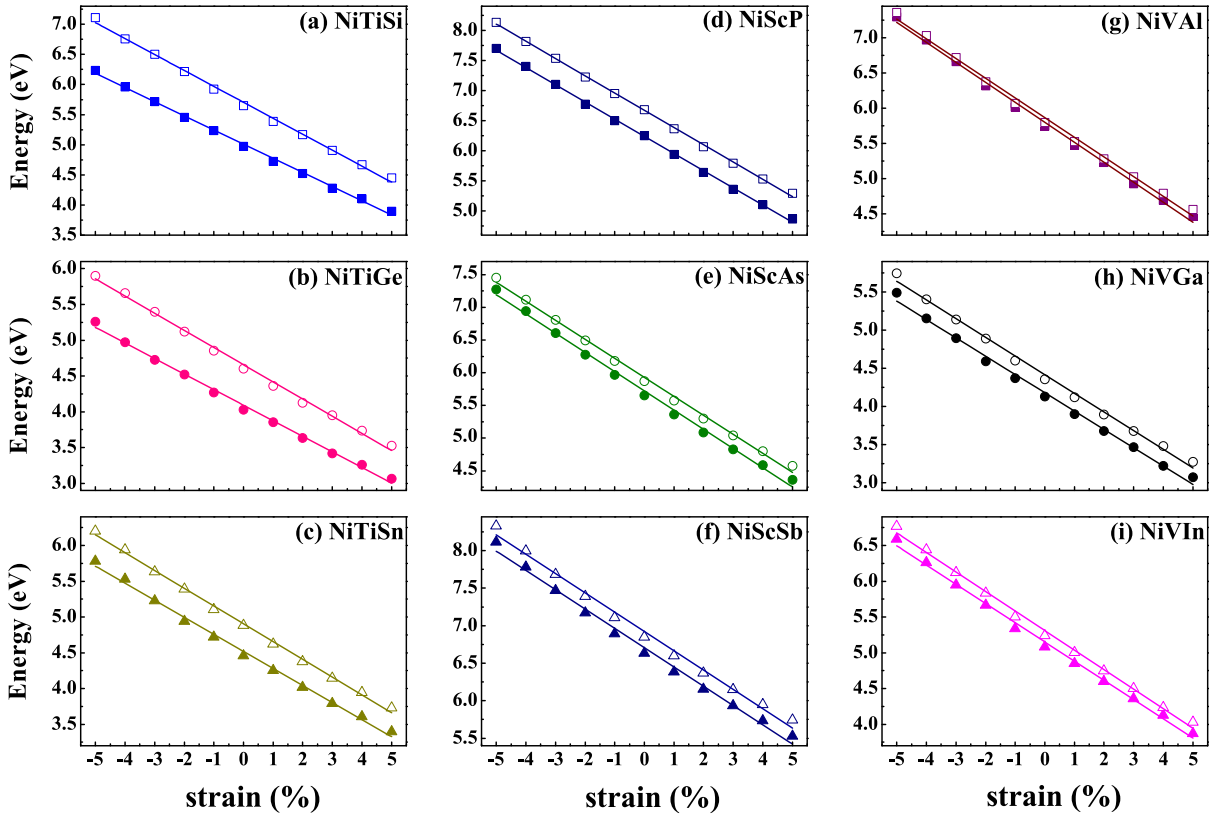

Figure 2. Band-edge energy vs the lattice strain for nine nickel-based compounds. The dots and solid lines are, respectively, the calculated results and fitted data.

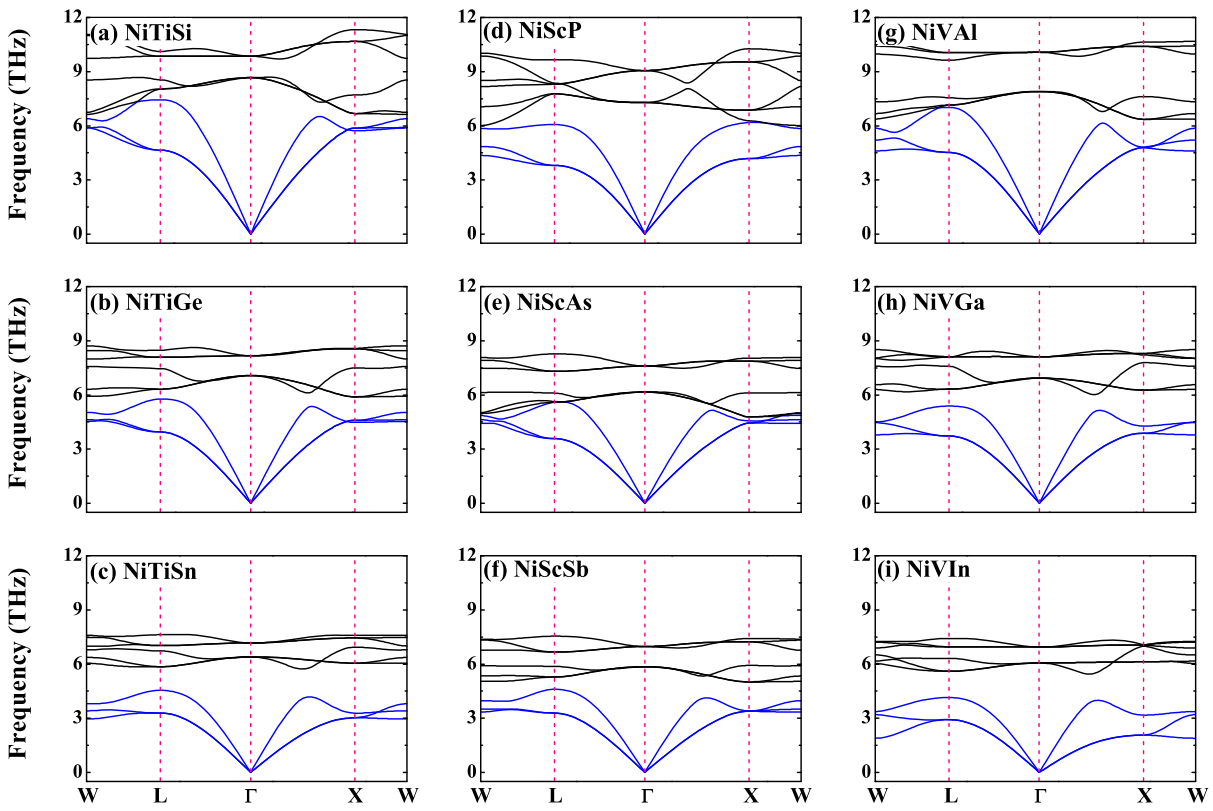

Figure 3. Calculated phonon band structure of NiYZ (Y = Ti, Sc, and V; Z = Si, Ge, Sn, P, As, Sb, Al, Ga, and In) in the half-Heusler structure.

distance from the convex hull provides a measure of thermodynamic stability. Accordingly, a compound is stable if its total energy distance to the convex hull is zero. Otherwise, a metastable compound should be within a range above the

https://doi.org/10.1021/acsomega.1c02172
ACS Omega 2021, 6, 18269−18280

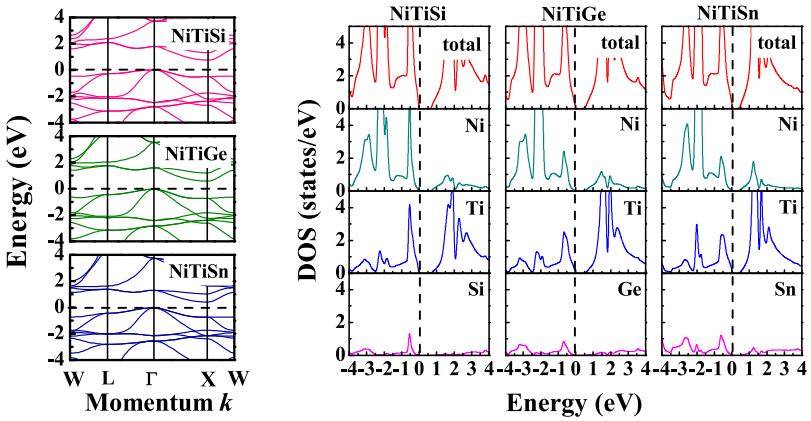

Figure 4. Band structure (left), total and atom-projected DOSs (right) for NiTiZ groups with Z = Si, Ge, or Sn. The dashed lines denote the Fermi levels.

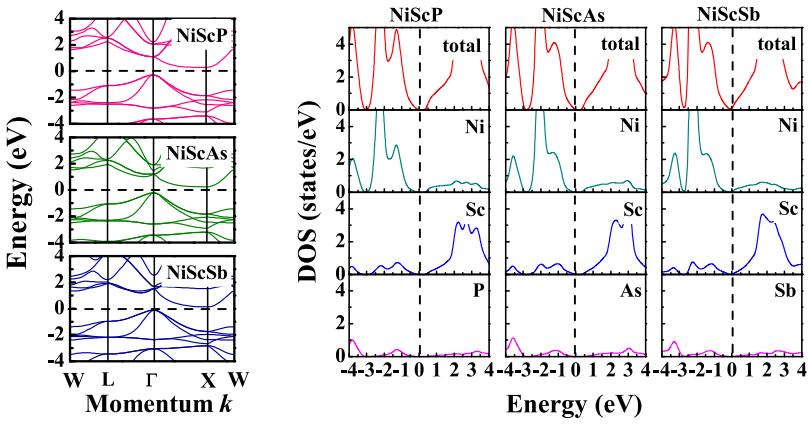

Figure 5. Band structure (left), total and atom-projected DOSs (right) for NiScZ groups with Z = P, As, or Sb. The dashed lines denote the Fermi levels.

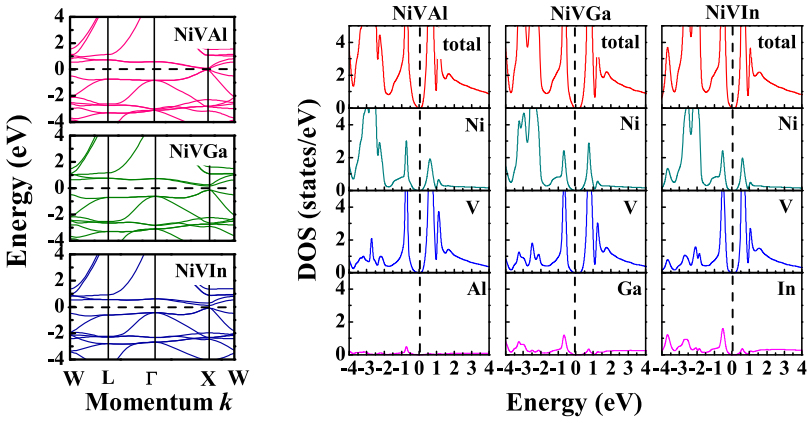

Figure 6. Band structure (left), total and atom-projected DOSs (right) for NiVZ groups with Z = Al, Ga, or In. The dashed lines denote the Fermi levels.

convex hull of formation energy. The available values of the distance from the convex hull for Ni-based compounds in $C1_b$ phase are listed in Table 1.[17] It is seen that some compounds are thermodynamically stable, and many others are quite close to the convex hull. We also note that our DFT calculations on Ni-based compounds are conducted at zero pressure and temperature. However, the unstable phases can also be experimentally realizable under carefully controlled conditions including high temperatures, high pressures, defects, and dopants.[31] On the other hand, Ceder et al. have proposed that metastable phases can exhibit superior properties than their corresponding stable phases by numerous materials technologies.[32] Therefore, we further explore the electronic and transport properties of NiYZ (Y = Ti, Sc, and V; Z = Si, Ge, Sn, P, As, Sb, Al, Ga, and In) in the $C1_b$ phase for their potential application as TE materials.

Electronic Structure and Effective Mass. We first plot the band structure and total and atom-projected DOSs for NiTiZ systems with Z = Si, Ge, or Sn in Figure 4. It can be seen that the minimum of the conduction band is located at

https://doi.org/10.1021/acsomega.1c02172
ACS Omega 2021, 6, 18269−18280

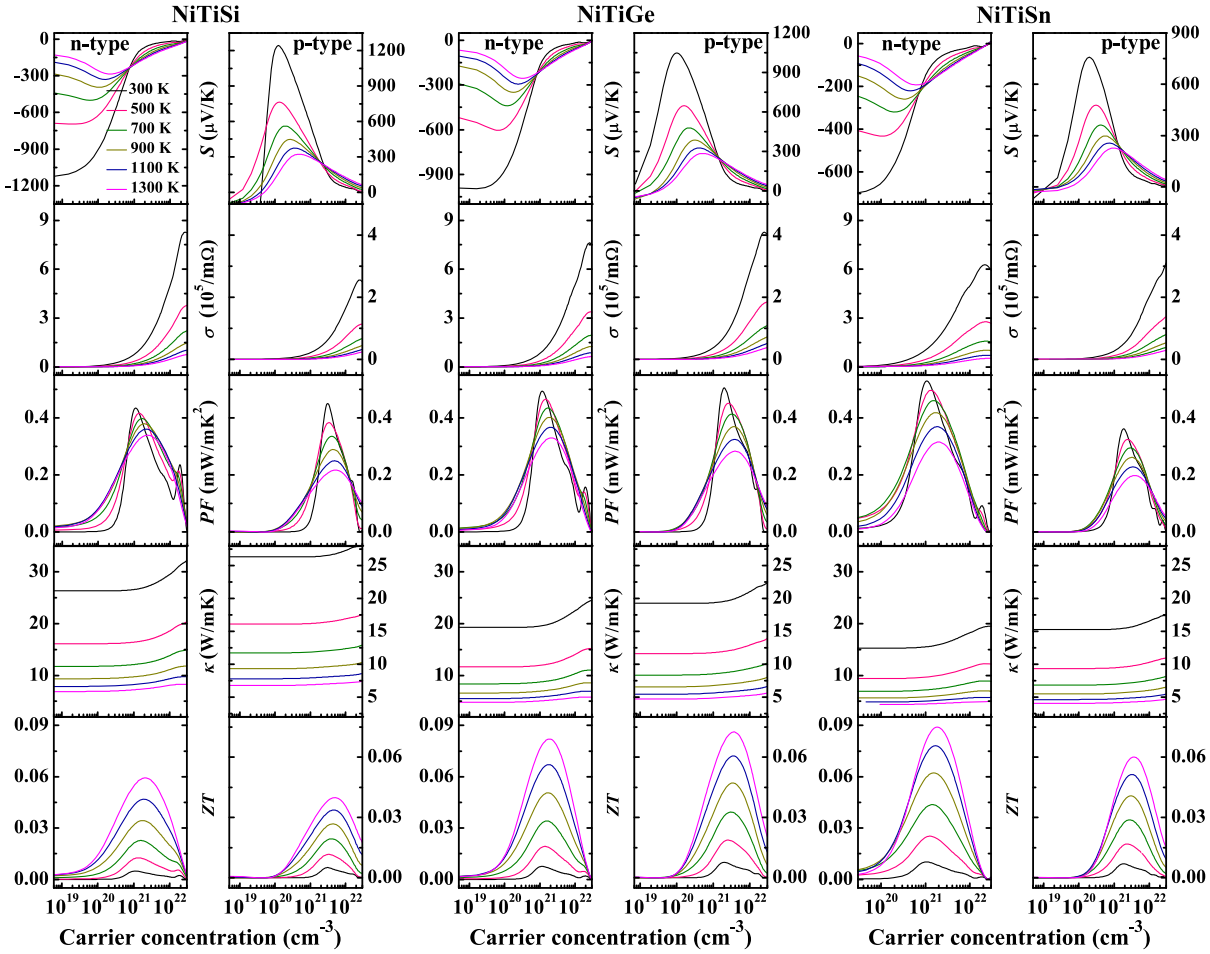

Figure 7. Carrier concentration dependence of the calculated Seebeck coefficient (S), electrical conductivity (σ), power factor (PF), thermal conductivity (κ), and figure of merit (ZT) for n-type and p-type NiTiZ (Z = Si, Ge, and Sn) systems at various temperatures.

the X point for all the three compounds. Otherwise, the maximum of their valence bands is at the Γ point, thus forming X−Γ indirect energy gaps. The flatter top of the valence band near E_f indicates a larger effective mass value for holes. This can also be observed from Table 2 that electrons hold a smaller effective mass than holes in NiTiZ (Z = Si, Ge, and Sn) groups. The energy gap is formed mainly by the d−d hybridization among Ni and Ti atoms.

Similarly, the band structure and the total and atom-projected DOSs for half-Heusler alloys NiScZ (Z = P, As, and Sb) with valence electrons of 18 are presented in Figure 5. The X−Γ indirect energy gap can also be observed, which is similar to that found in the above-mentioned NiTi-based half-Heusler semiconductors. The smallest energy gap among the three NiSc-based materials is calculated to be 0.207 eV for NiScSb. We point out that the valence band edge in NiScZ (Z = P, As, and Sb) groups is much steeper than that of the conduction band near the E_f. Therefore, the effective mass of electrons exhibits relatively larger values than those of holes. It can also be found that the slope near the valence band edge in the DOS is much sharper than that near the conduction band edge. As a result, NiScZ (Z = P, As, and Sb) may have a large power factor when used as p-type semiconductors for TE applications.

Figure 6 shows the band structure and the DOS for NiVZ (Z = Al, Ga, and In). The band structure of these three systems is greatly different from other six half-Heusler semiconductors. The VBM and the CBM for NiVZ (Z = Al, Ga, and In) just form direct energy gaps at the X point near the Fermi level. It is noted that the band gaps of NiVAl, NiVGa, and NiVIn are, respectively, 0.091, 0.286, and 0.264 eV, which are similar to the available results.[17] Furthermore, the DOS show a sharp slope around the Fermi level, which are the predictions for high-power factors. As a result, half-Heusler semiconductors NiVZ (Z = Al, Ga, and In) are expected to be good TE materials. The DOS effective mass m^* is obtained via $m^* = N_v^{2/3} m_b^*$,[33] in which N_v and m_b^* are the number of degenerate carrier pockets and the band effective mass. The average band effective mass of electrons (holes) shown in Table 2 is determined by the dispersion curve at the CBM. For NiTi- and NiSc-based half-Heusler, the band effective mass of holes is the average between the values of band effective mass, respectively, along the Γ−L and Γ−X directions. The VBM of NiTi- and NiSc-based half-Heusler compounds is located at the Γ point with a band degeneracy of $N_v = 3$.[34] The N_v is also 3 for the CBM with one band at the X point. In comparison, the VBM of NiV-based half-Heusler lies in point X with a higher band degeneracy of $N_v = 6$,[35] which is beneficial to a sharp slope of DOS near the Fermi level, thus resulting in a large DOS effective mass without deterioration of μ. Therefore, the high band degeneracy N_v for the VBM implies that NiV-based half-Heusler is a good p-type TE material. The relaxation time for electrons and holes in those nine half-Heusler semiconductors is predicted and listed in Table 2.

https://doi.org/10.1021/acsomega.1c02172
ACS Omega 2021, 6, 18269−18280

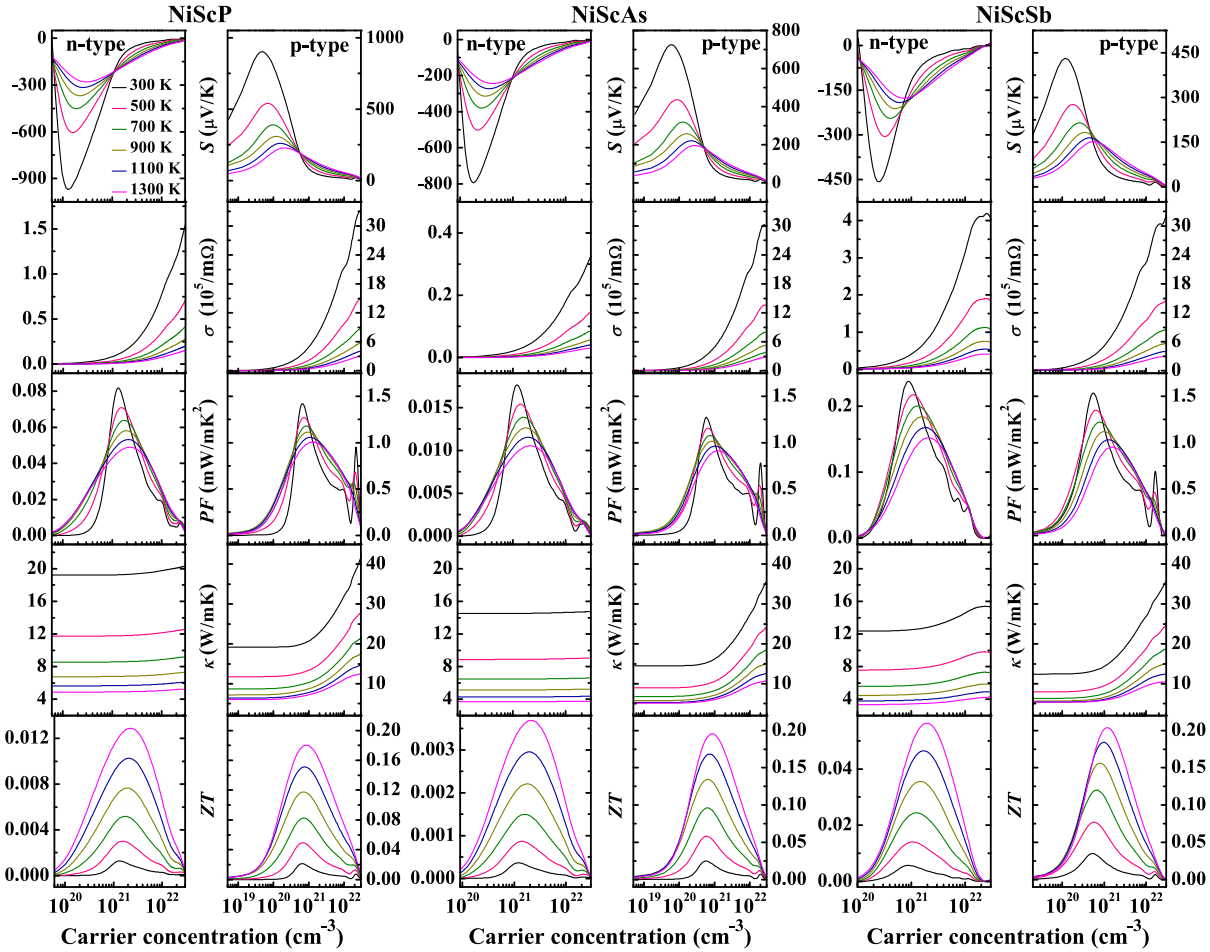

Figure 8. Carrier concentration dependence of the calculated Seebeck coefficient (S), electrical conductivity (σ), power factor (PF), thermal conductivity (κ), and figure of merit (ZT) for n-type and p-type NiScZ (Z = P, As, and Sb) systems at various temperatures.

TE Properties. We now focus on TE properties by discussing the Seebeck coefficient, electrical conductivity, power factor, thermal conductivity, and figure of merit. The variation of transport parameters (S, σ, PF, κ, and ZT) with the carrier concentration (n) for both n-type and p-type NiTiZ (Z = Si, Ge, and Sn) when the temperature (T) increases from 300 to 1300 K is shown in Figure 7. It is obvious that the value of S for p-type first increases to a maximum as a function of the carrier concentration and then decreases with increasing n. However, the Seebeck coefficient exhibits different variations for n-type. We find that the maximal value of S at low temperatures is much larger than that at higher temperatures for both p-type and n-type systems at the same carrier concentration. It is clear that the electrical conductivity of the n-type NiTi-based half-Heusler compounds is much larger than that of p-type ones at the same carrier concentration and temperature. There is a sharp increase of the power factor as the carrier concentration ranges from 10^{20} to 10^{22} cm^{-3}. We also find that the electrical conductivity decreases with increased temperature because of $\sigma = ne\mu$. The carrier mobility μ can be derived from DP theory. In this case, the carrier mobility is inversely proportional to temperature. Therefore, enhanced temperature will lead to a reduced carrier mobility, thus resulting in a decreased electrical conductivity at a certain carrier concentration. The decreased electrical conductivity will further decrease the power factor as the temperature increases due to PF = $S^2\sigma$. The same phenomenon can also be found in another work.[21] By adding the calculated lattice thermal conductivity (κ_l) to the obtained electronic thermal conductivity (κ_e) from the BoltzTraP code, the total thermal conductivity (κ) as a function of carrier concentration at different temperatures is presented in Figure 6. As evident from the figure, the curves first remain gentle with n and then rise with a further increase in n. The n-type systems are seen to hold a low thermal conductivity rather than p-type systems. As a result, for n-type NiTiZ (Z = Si, Ge, and Sn) half-Heusler semiconductors at each temperature, the figure of merit is larger than that for p-type systems.

The carrier concentration dependence of relevant quantities of NiScZ (Z = P, As, and Sb) is plotted in Figure 8. It is noted that the variation of the Seebeck coefficient and the power factor with n is basically the same as that shown in Figure 7. However, the calculated PF values are greatly enhanced for p-type systems but much smaller than that for n-type systems compared to the corresponding doping level in NiTiZ (Z = Si, Ge, and Sn) groups. On the other hand, the values of PF for p-type NiScZ (Z = P, As, and Sb) are much larger than those for n-type ones at the same temperature, resulting in higher ZT values for p-type systems in spite of the lower thermal conductivity found in n-type systems. The optimal value of ZT at T = 1300 K is 0.204 for p-type NiScSb at the carrier concentration of 1.189×10^{21} cm^{-3}. NiScSb is promising for TE applications.

https://doi.org/10.1021/acsomega.1c02172
ACS Omega 2021, 6, 18269−18280

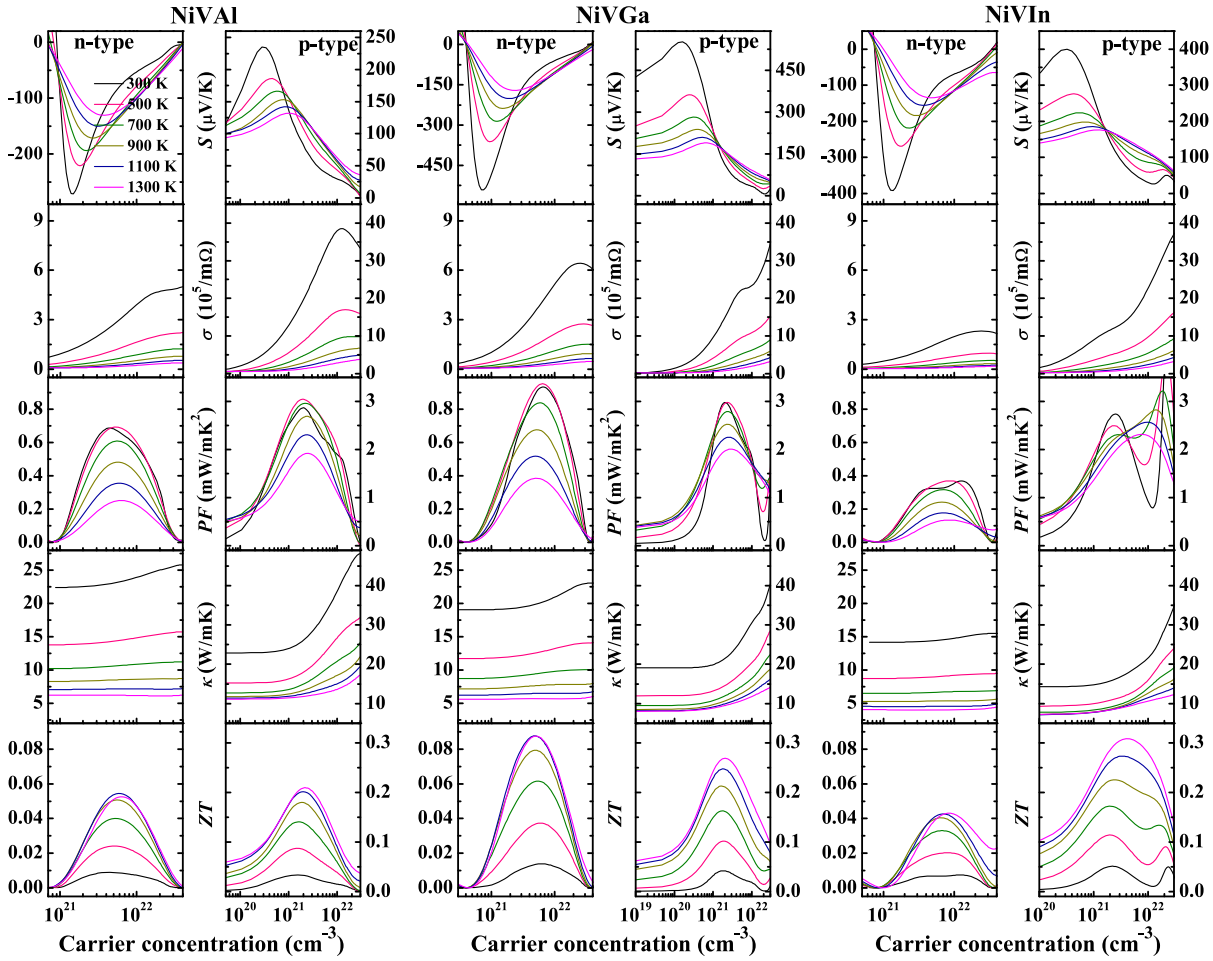

Figure 9. Carrier concentration dependence of the calculated Seebeck coefficient (S), electrical conductivity (σ), power factor (PF), thermal conductivity (κ), and figure of merit (ZT) for n-type and p-type NiVZ (Z = Al, Ga, and In) systems at various temperatures.

In Figure 9, we plot the Seebeck coefficient, electrical conductivity, power factor, thermal conductivity, and the figure of merit as the carrier concentration varies in the temperature range of 300−1300 K for NiVZ (Z = Al, Ga, and In) with both n- and p-type systems. The behavior of S for these three half-Heusler compounds shows a similar trend as seen in Figures 7 and 8. The behavior of electrical conductivity for NiSc- and NiV-based half-Heusler compounds is, however, completely different from that for NiTi-based compounds. It is the p-type systems that hold larger electrical conductivity. The discrepancy is caused by the obvious difference between the relaxation time of electrons and holes. On the other hand, the electrical conductivity of NiV-based half-Heusler compounds is much larger in comparison with that of NiTi- and NiSc-based compounds at an optimal carrier concentration due to the smaller value of the band gap (making it easier for thermally excited electrons reaching the conduction bands), hence giving a larger power factor of NiV-based half-Heusler compared to the others systems in this study. Thus, in spite of having the lowest Seebeck coefficient, NiV-based half-Heusler has the highest power factor due to the largest electrical conductivity. The power factor versus the carrier concentration for n-type first increases up to maximal values of 0.691 mW m^{-1} K^{-2} for NiVAl, 0.952 mW m^{-1} K^{-2} for NiVGa at T = 500 K, and 0.368 mW m^{-1} K^{-2} for NiVIn at T = 300 K. Then, it decreases with further increasing n. For p-type systems, the power factor can be optimized to as high as 3.044 mW m^{-1} K^{-2} for NiVAl, 2.979 mW m^{-1} K^{-2} for NiVGa at T = 500 K and 5.152 mW m^{-1} K^{-2} for NiVIn at T = 300 K, which are much larger compared to values obtained for other promising half-Heusler TE materials, such as ZrNiSn (3.4 mW m^{-1} K^{-2}),[9] TiCoSb (2.3 mW m^{-1} K^{-2}),[36] TiNiSn (1.5 mW m^{-1} K^{-2}), and doped $Ti_{0.5}Zr_{0.5}NiSn$ (1.8 mW m^{-1} K^{-2}).[37] Looking at the variation of κ as a function of carrier concentration, it shows a descending trend for n-type and p-type NiVZ (Z = Al, Ga, and In) compounds as the temperature increases from 300 K. Notably, the ZT values for both n-type and n-type NiVZ (Z = Al, Ga, and In) exceed those of NiTiZ (Z = Si, Ge, and Sn) and NiScZ (Z = P, As, and Sb) semiconductors, which is mainly attributed to the nature of the band structures seen in Figure 6. For p-type systems at 1300 K, the highest ZT values of 0.210 for NiVAl, 0.269 for NiVGa, and 0.309 for NiVIn are obtained. The obtained maximum ZT values are much larger than that in good TE half-Heusler compounds NbCoSn,[38] TiCoSb,[8] and ZrNiSn.[9] In this study, we obtain the TE properties based on the relaxation time determined by the DP theory and effective mass approximation, which is accurate to produce relaxation time for FeNbSb-based half-Heusler material compared to experiments.[21] Their work indicates that the calculated electrical conductivity is a little higher than the experimental value of $FeNb_{1-x}Ti_xSb$ (x = 0.04, 0.06, and 0.08) at low temperatures, resulting in the larger calculated ZT value than the measured one. This discrepancy can be partially attributed to other scattering mechanisms (grain boundary scattering,

https://doi.org/10.1021/acsomega.1c02172
ACS Omega 2021, 6, 18269−18280

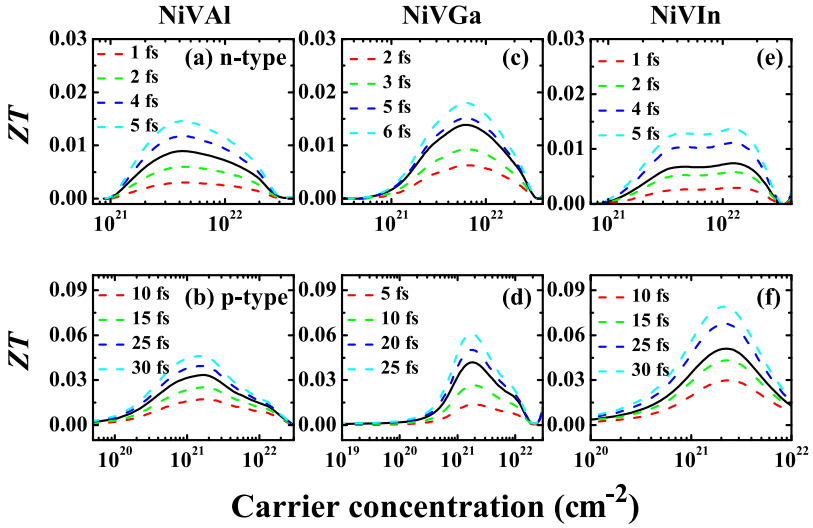

Figure 10. Calculated ZT of half-Heusler NiVZ (Z = Al, Ga, and In) at 300 K as a function of carrier concentration with different relaxation times.

impurity scattering, other defect scattering, and so on), which cannot be neglected at low temperatures. As the temperature goes high, there exists a good agreement between the calculated and measured electrical conductivity, indicating that the carrier scattering can be safely ignored. On the other hand, the microstructures and associated defects of the experimental sample will have a substantial effect on the TE properties. The theoretical descriptions for the complicated scattering processes are difficult. Hence, if we consider the theoretical approximations and the uncertainties in the experiment, the calculated results are in reasonable and acceptable agreement with the experimental results. However, the DP model produces reasonable relaxation time based on the electron−acoustic−phonon interactions. However, the full ignorance of electron−optical−phonon interactions, polar scattering, and other scattering mechanisms in this model may give rise to the possible uncertainties in the calculated relaxation time.[39] To make a comparison to the ZT values of promising TE materials, we also plot the ZT values of half-Heusler NiVZ (Z = Al, Ga, and In) at 300 K with a relaxation time range centered around the calculated ones from the DP model in Figure 10. The solid black lines stand for the ZT using the relaxation time obtained from the DP model. Assuming the same relaxation time, our obtained values of ZT are even larger than those of the previously promising TE material such as half-Heusler FeNbSb.[21] As a result, this study predicts the promising TE performance of nine nickel based half-Heusler semiconductors, especially NiVAl, NiVGa, and NiVIn when used as potential candidate matrices for TE nanocomposites.

■ CONCLUSIONS

In recent years, considerable efforts have been made to enhance the TE efficiency of the half-Heusler semiconductors by forming nanocomposites, nanostructuring, and isoelectronic alloying. This improvement, however, depends a lot on the high ZT values of the parent ideal compounds. With the aim of finding new parent half-Heusler compounds, we selected nine nickel-based half-Heusler semiconductors NiXY (X = Ti, Sc, and V; Y = Si, Ge, Sn, P, As, Sb, Al, Ga, and In) to conduct detailed electronic structure and TE properties' calculations based on DFT in combination with the semi-classical Boltzmann theory. Their ground-state structures are fully optimized and compared with theoretical results, with good agreement observed. The calculated elastic constants and phonon spectra verified their mechanical and dynamical stability. The observed sharper slope of DOS near the Fermi level in NiVAl, NiVGa, and NiVIn manifests a higher effective mass and gives rise to higher ZT values at high temperatures. At T = 1300 K, the ZT values can be as high as 0.210, 0.269, and 0.309, respectively, for p-type NiVAl, NiVGa, and NiVIn, and they can be used as promising candidate matrices for high-performance TE nanocomposites. Our detailed work on nine nickel-based half-Heusler semiconductors certainly shines a light and provides guidance for future experimental works.

■ COMPUTATIONAL METHOD AND PROCESS

Our first-principles calculations are conducted within the Vienna ab initio simulation package[40−42] using the projector augmented wave method.[43] The electronic exchange−correlation functional is solved by the generalized gradient approximation with the Perdew−Burke−Ernzerhof functional.[44] The plane-wave cutoff energy and Monkhorst−Pack uniform k-point sampling are, respectively, selected as 520 eV and 15 × 15 × 15 based on strict convergence tests. The self-consistency tolerance is set to 10^{-6} eV for the energy error and 0.01 eV/Å for the force on each atom. Our DFT calculations are performed on the nine Ni-based half-Heusler compounds NiYZ (Y = Ti, Sc, and V; Z = Si, Ge, Sn, P, As, Sb, Al, Ga, and In). The $3d^84s^2$ is considered as the valence state of Ni. In NiYZ, Y represents the Ti ($3d^24s^2$) element and the Z groups are Si ($3s^23p^2$), Ge ($4s^24p^2$), and Sn ($5s^25p^2$). The number of valence electrons for Sc ($3d^14s^2$) is one less than that for Ti. Therefore, the P ($3s^23p^3$), As ($4s^24p^3$), and Sb ($5s^25p^3$) groups hold one more electron than the Si groups. For V, the valence state is chosen as $3d^34s^2$, and the valence states for Al, Ga, and In are, respectively, $3s^23p^1$, $4s^24p^1$, and $5s^25p^1$. As a result, the obtained three Ni-based half-Heusler groups NiTiZ (Z = Si, Ge, and Sn), NiScZ(Z = P, As, and Sb), and NiVZ (Z = Al, Ga, and In) are all with 18 total valence electrons per unit cell. To check the dynamical stability of the NiYZ (Y = Ti, Sc, and V; Z = Si, Ge, Sn, P, As, Sb, Al, Ga, and In) crystallized in the half-Heusler structure, we calculate their phonon spectra using a small displacement method, as implemented in the PHONO-

https://doi.org/10.1021/acsomega.1c02172
ACS Omega 2021, 6, 18269−18280

PY code.[45] In the present case, the force constant matrix is obtained based on slight displacement of atoms in a 3 × 3 × 3 supercell. A 5 × 5 × 5 uniform mesh is employed. Transport properties are then calculated based on the electronic band structure obtained on a highly dense 25 × 25 × 25 k-point mesh by the semi-classical Boltzmann transport theory, as implemented in the BoltzTraP code.[46] In this approach, one can obtain the Seebeck coefficient, electrical conductivity, and electronic thermal conductivity. However, the values of electrical conductivity and electronic thermal conductivity are both dependent on the relaxation time (τ). To get accurate predictions for TE materials, we have to calculate the relaxation time and lattice thermal conductivity (κ_l). In our study, the τ value as a function of temperature is determined with the help of DP theory and effective mass approximation. As the lattice constant is much smaller than the wavelength of thermally activated carriers, the electron-acoustic phonon coupling is therefore dominant in the scattering of carriers.[47] The scheme is fortunately simplified. Accordingly, the formula of the carrier relaxation time for a three-dimensional system is

$$\tau = \frac{2\sqrt{2\pi}C\hbar^4}{3(k_B T m^*)^{3/2} {E_1}^2} \tag{1}$$

The elastic constant C can be calculated as

$$C = \frac{1}{V_0}\frac{\partial^2 E}{\partial(\Delta l/l_0)^2} \tag{2}$$

where V_0 and E stand for the volume of the equilibrium unit cell and the total energy of the system. l_0 is the optimized lattice constant, whereas $\Delta l = l - l_0$ is the lattice constant variation. m^* is the effective mass and is obtained from the accurate band structure. E_1 is the DP constant defined as

$$E_1 = \frac{\partial E_{\text{edge}}}{\partial(\Delta l/l_0)} \tag{3}$$

which represents the energy change in VBM or CBM per unit strain. All of the three quantities (C, m^*, and E_1) are readily obtained based on the first-principles calculation. The lattice thermal conductivity is obtained based on DFT calculations within the Debye−Callaway model,[48] which produces reliable results compared to the experiment.[49] In this approach, κ_l is modeled as simple descriptors including the acoustic ($\kappa_{l,ac}$) and optical phonon modes ($\kappa_{l,op}$).[50] The predominant contribution stems from the acoustic phonon, which is described as

$$\kappa_{l,ac} = \frac{(6\pi^2)^{2/3}}{4\pi^2}\frac{\bar{M}V_s^3}{TV^{2/3}\gamma^2 n^{1/3}} \tag{4}$$

and the optical phonon mode is in the form of

$$\kappa_{l,op} = \frac{3k_B V_s}{2V^{2/3}}\left(\frac{\pi}{6}\right)^{1/3}\left(1 - \frac{1}{n^{2/3}}\right) \tag{5}$$

In the formula, $\bar{M}$ and V are the average mass and volume per atom, respectively. Here, n is the number of atoms in the primitive cell. The Grüneisen parameter (γ) reflecting the relationship of the phonon frequency with the crystal volume change is calculated by employing the quasi-harmonic Debye model.[51] V_s is the velocity of sound and approximates to be $V_s \simeq \sqrt{B/d}$, where B is the bulk modulus and d is the density. All these parameters can be obtained from ground-state calculations. We note that the calculated κ_l for NiTiSn is 15.26 W m^{-1} K^{-1} at 300 K, which is similar to 15.4 W m^{-1} K^{-1} (at T = 300 K) found in Andrea's work,[23] thus suggesting the reliability of the method in this work.

■ AUTHOR INFORMATION

Corresponding Authors

Zhibin Shao − *School of Physics and Information Technology, Shaanxi Normal University, Xi'an 710119, China*; Email: zhibin_shao@snnu.edu.cn

Haiping Lin − *School of Physics and Information Technology, Shaanxi Normal University, Xi'an 710119, China; Institute of Functional Nano & Soft Materials, Jiangsu Key Laboratory for Carbon-Based Functional Materials & Devices, Collaborative Innovation Center of Suzhou Nano Science and Technology, Soochow University, Suzhou 215123, China*; Email: hplin@suda.edu.cn

Minghu Pan − *School of Physics and Information Technology, Shaanxi Normal University, Xi'an 710119, China*; orcid.org/0000-0002-1520-209X; Email: minghupan@snnu.edu.cn

Authors

Xiaorui Chen − *School of Physics and Information Technology, Shaanxi Normal University, Xi'an 710119, China*

Xin Zhang − *School of Physics, Northwest University, Xi'an 710127, China*

Jianzhi Gao − *School of Physics and Information Technology, Shaanxi Normal University, Xi'an 710119, China*

Qing Li − *School of Physics and Information Technology, Shaanxi Normal University, Xi'an 710119, China; Institute of Functional Nano & Soft Materials, Jiangsu Key Laboratory for Carbon-Based Functional Materials & Devices, Collaborative Innovation Center of Suzhou Nano Science and Technology, Soochow University, Suzhou 215123, China*

Complete contact information is available at: https://pubs.acs.org/10.1021/acsomega.1c02172

Notes

The authors declare no competing financial interest.

■ ACKNOWLEDGMENTS

We acknowledge the support from the National Natural Science Foundation of China (nos. 91745115, 21771134, 21972083, and 12004234), the Natural Science Basic Research Program of Shaanxi (no. 2021JQ-297), and the Postdoctoral Innovative Talent Support Program of China (no. BX20200202).

■ REFERENCES

(1) DiSalvo, F. J. Thermoelectric cooling and power generation. *Science* **1999**, *285*, 703−706.

(2) Gahlawat, S.; He, R.; Chen, S.; Wheeler, L.; Ren, Z. F.; White, K. W. Elastic constants determined by nanoindentation for p-type thermoelectric half-Heusler. *J. Appl. Phys.* **2014**, *116*, 083516.

(3) Nolas, G. S.; Poon, J.; Kanatzidis, M. Recent developments in bulk thermoelectric materials. *MRS Bull.* **2006**, *31*, 199−205.

(4) Chen, S.; Ren, Z. Recent progress of half-Heusler for moderate temperature thermoelectric applications. *Mater. Today* **2013**, *16*, 387−395.

(5) Yan, X.; Liu, W.; Chen, S.; Wang, H.; Zhang, Q.; Chen, G.; Ren, Z. Thermoelectric property study of nanostructured p-type half-

Heuslers (Hf, Zr, Ti)$CoSb_{0.8}Sn_{0.2}$. *Adv. Energy Mater.* **2013**, *3*, 1195−1200.
(6) Yan, X.; Liu, W.; Wang, H.; Chen, S.; Shiomi, J.; Esfarjani, K.; Wang, H.; Wang, D.; Chen, G.; Ren, Z. Stronger phonon scattering by larger differences in atomic mass and size in p-type half-Heuslers $Hf_{1-x}Ti_xCoSb_{0.8}Sn_{0.2}$. *Energy Environ. Sci.* **2012**, *5*, 7543−7548.
(7) Liu, Y.; Xie, H.; Fu, C.; Snyder, G. J.; Zhao, X.; Zhu, T. Demonstration of phonon-glass electron-crystal strategy in (Hf,Zr)-NiSn half-Heusler thermoelectric materials by alloying. *J. Mater. Chem. A* **2015**, *3*, 22716−22722.
(8) Xia, Y.; Ponnambalam, V.; Bhattacharya, S.; Pope, A. L.; Poon, S. J.; Tritt, T. M. Electrical transport properties of TiCoSb half-Heusler phases that exhibit high resistivity. *J. Phys.: Condens. Matter* **2001**, *13*, 77−89.
(9) Shen, Q.; Chen, L.; Goto, T.; Hirai, T.; Yang, J.; Meisner, G. P.; Uher, C. Effects of partial substitution of Ni by Pd on the thermoelectric properties of ZrNiSn-based half-Heusler compounds. *Appl. Phys. Lett.* **2001**, *79*, 4165−4167.
(10) Yu, C.; Zhu, T.-J.; Shi, R.-Z.; Zhang, Y.; Zhao, X.-B.; He, J. High-performance half-Heusler thermoelectric materials $Hf_{1-x}Zr_xNiSn_{1-y}Sb_y$ prepared by levitation melting and spark plasma sintering. *Acta Mater.* **2009**, *57*, 2757−2764.
(11) Chen, L.; Gao, S.; Zeng, X.; Mehdizadeh Dehkordi, A.; Tritt, T. M.; Poon, S. J. Uncovering high thermoelectric figure of merit in (Hf,Zr)NiSn half-Heusler alloys. *Appl. Phys. Lett.* **2015**, *107*, 041902.
(12) Sakurada, S.; Shutoh, N. Effect of Ti substitution on the thermoelectric properties of (Zr,Hf)NiSn half-Heusler compounds. *Appl. Phys. Lett.* **2005**, *86*, 082105.
(13) Zhu, T.; Fu, C.; Xie, H.; Liu, Y.; Zhao, X. High efficiency half-Heusler thermoelectric materials for energy harvesting. *Adv. Energy Mater.* **2015**, *5*, 1500588.
(14) Fu, C.; Zhu, T.; Liu, Y.; Xie, H.; Zhao, X. Band engineering of high performance p-type FeNbSb based half-Heusler thermoelectric materials for figure of merit zT > 1. *Energy Environ. Sci.* **2015**, *8*, 216−220.
(15) Fu, C.; Bai, S.; Liu, Y.; Tang, Y.; Chen, L.; Zhao, X.; Zhu, T. Realizing high figure of merit in heavy-band p-type half-Heusler thermoelectric materials. *Nat. Commun.* **2015**, *6*, 8144.
(16) Fu, C.; Wu, H.; Liu, Y.; He, J.; Zhao, X.; Zhu, T. Enhancing the figure of merit of heavy-band thermoelectric materials through hierarchical phonon scattering. *Adv. Sci.* **2016**, *3*, 1600035.
(17) Ma, J. H.; Hegde, V. I.; Munira, K.; Xie, Y. K.; Keshavarz, S.; Mildebrath, D. T.; Wolverton, C.; Ghosh, A. W.; Butler, W. H. Computational investigation of half-Heusler compounds for spin-tronics applications. *Phys. Rev. B* **2017**, *95*, 024411.
(18) de F Pereira, A. F. F.; de Souza, S. M.; Ghosh, A. Analysis of structural and electronic properties of NiTiZ (Z = Si, Ge, Sn and Sb) under high-pressure using ab initio calculations. *Mater. Today Commun.* **2020**, *25*, 101613.
(19) Jaishi, D. R.; Sharma, N.; Karki, B.; Belbase, B. P.; Adhikari, R. P.; Ghimire, M. P. Electronic structure and thermoelectric properties of half-Heusler alloys NiTZ. *AIP Adv.* **2021**, *11*, 025304.
(20) Hung, N. T.; Nugraha, A. R. T.; Saito, R. Two-dimensional InSe as a potential thermoelectric material. *Appl. Phys. Lett.* **2017**, *111*, 092107.
(21) Hong, A. J.; Li, L.; He, R.; Gong, J. J.; Yan, Z. B.; Wang, K. F.; Liu, J.-M.; Ren, Z. F. Full-scale computation for all the thermoelectric property parameters of half-Heusler compounds. *Sci. Rep.* **2016**, *6*, 22778.
(22) Shi, F.; Si, M. S.; Xie, J.; Mi, K.; Xiao, C.; Luo, Q. Hybrid density functional study of bandgaps for 27 new proposed half-Heusler semiconductors. *J. Appl. Phys.* **2017**, *122*, 215701.
(23) Andrea, L.; Hug, G.; Chaput, L. Ab initio phonon properties of half-Heusler NiTiSn, NiZrSn and NiHfSn. *J. Phys.: Condens. Matter* **2015**, *27*, 425401.
(24) Roy, A.; Bennett, J. W.; Rabe, K. M.; Vanderbilt, D. Half-Heusler semiconductors as piezoelectrics. *Phys. Rev. Lett.* **2012**, *109*, 037602.
(25) Hermet, P.; Niedziolka, K.; Jund, P. A first-principles investigation of the thermodynamic and mechanical properties of Ni-Ti-Sn Heusler and half-Heusler materials. *RSC Adv.* **2013**, *3*, 22176−22184.
(26) Miao, M. S.; Prikhodko, M.; Lambrecht, W. R. L. Changes of the geometry and band structure of SiC along the orthorhombic high-pressure transition path between the zinc-blende and rocksalt structures. *Phys. Rev. B: Condens. Matter Mater. Phys.* **2002**, *66*, 064107.
(27) Sin'ko, G. V.; Smirnov, N. A. Ab initio calculations of elastic constants and thermodynamic properties of bcc, fcc, and hcp Al crystals under pressure. *J. Phys.: Condens. Matter* **2002**, *14*, 6989−7005.
(28) Yip, S.; Li, J.; Tang, M.; Wang, J. Mechanistic aspects and atomic-level consequences of elastic instabilities in homogeneous crystals. *Mater. Sci. Eng., A* **2001**, *317*, 236−240.
(29) Wu, Z.-j.; Zhao, E. J.; Xiang, H. P.; Hao, X. F.; Liu, X. J.; Meng, J. Crystal structures and elastic properties of superhard IrN_2 and IrN_3 from first principles. *Phys. Rev. B: Condens. Matter Mater. Phys.* **2007**, *76*, 054115.
(30) Frantsevich, I. N.; Voronov, F. F.; Bokuta, S. A. *Elastic Constants and Elastic Moduli of Metals and Insulators Handbook*, 60; Franstsevich, I. N., Eds.; Naukova Dumka: Kiev, 1983.
(31) Cerqueira, T. F. T.; Lin, S.; Amsler, M.; Goedecker, S.; Botti, S.; Marques, M. A. L. Identification of novel Cu, Ag, and Au ternary oxides from global structural prediction. *Stl. Chem. Mater* **2015**, *27*, 4562−4573.
(32) Sun, W.; Dacek, S. T.; Ong, S. P.; Hautier, G.; Jain, A.; Richards, W. D.; Gamst, A. C.; Persson, K. A.; Ceder, G. The thermodynamic scale of inorganic crystalline metastability. *Sci. Adv.* **2016**, *2*, e1600225.
(33) Pei, Y.; LaLonde, A. D.; Wang, H.; Snyder, G. J. Low effective mass leading to high thermoelectric performance. *Energy Environ. Sci.* **2012**, *5*, 7963−7969.
(34) Li, S.; Zhao, H.; Li, D.; Jin, S.; Gu, L. Synthesis and thermoelectric properties of half-Heusler alloy YNiBi. *J. Appl. Phys.* **2015**, *117*, 205101.
(35) Fang, T.; Zheng, S.; Chen, H.; Cheng, H.; Wang, L.; Zhang, P. Electronic structure and thermoelectric properties of p-type half-Heusler compound NbFeSb: a first-principles study. *RSC Adv.* **2016**, *6*, 10507−10512.
(36) Wu, T.; Jiang, W.; Li, X.; Zhou, Y.; Chen, L. Thermoelectric properties of p-type Fe-doped TiCoSb half-Heusler compounds. *J. Appl. Phys.* **2007**, *102*, 103705.
(37) Downie, R. A.; MacLaren, D. A.; Bos, J.-W. G. Thermoelectric performance of multiphase XNiSn (X = Ti, Zr, Hf) half-Heusler alloys. *J. Mater. Chem. A* **2014**, *2*, 6107−6114.
(38) Kimura, Y.; Tamura, Y.; Kita, T. Thermoelectric properties of directionally solidified half-Heusler compound NbCoSn alloys. *Appl. Phys. Lett.* **2008**, *92*, 012105.
(39) Liao, B.; Zhou, J.; Qiu, B.; Dresselhaus, M. S.; Chen, G. Ab initio study of electron-phonon interaction in phosphorene. *Phys. Rev. B: Condens. Matter Mater. Phys.* **2015**, *91*, 235419.
(40) Kresse, G.; Hafner, J. Ab initio molecular dynamics for liquid metals. *Phys. Rev. B: Condens. Matter Mater. Phys.* **1993**, *47*, 558−561.
(41) Kresse, G.; Hafner, J. Ab initio molecular-dynamics simulation of the liquid-metal-amorphous-semiconductor transition in germanium. *Phys. Rev. B: Condens. Matter Mater. Phys.* **1994**, *49*, 14251−14269.
(42) Kresse, G.; Furthmüller, J. Efficiency of ab-initio total energy calculations for metals and semiconductors using a plane-wave basis set. *Comput. Mater. Sci.* **1996**, *6*, 15−50.
(43) Blöchl, P. E. Projector augmented-wave method. *Phys. Rev. B: Condens. Matter Mater. Phys.* **1994**, *50*, 17953.
(44) Perdew, J. P.; Burke, K.; Ernzerhof, M. Generalized gradient approximation made simple. *Phys. Rev. Lett.* **1996**, *77*, 3865−3868.
(45) Alfè, D. PHON: A program to calculate phonons using the small displacement method. *Comput. Phys. Commun.* **2009**, *180*, 2622−2633.

https://doi.org/10.1021/acsomega.1c02172
ACS Omega 2021, 6, 18269−18280

(46) Madsen, G. K. H.; Singh, D. J. BoltzTraP A code for calculating band-structure dependent quantities. *Comput. Phys. Commun.* **2006**, *175*, 67−71.
(47) Cai, Y.; Zhang, G.; Zhang, Y.-W. Polarity-reversed robust carrier mobility in monolayer MoS_2 nanoribbons. *J. Am. Chem. Soc.* **2014**, *136*, 6269−6275.
(48) Callaway, J. Model for lattice thermal conductivity at low temperatures. *Phys. Rev.* **1959**, *113*, 1046−1051.
(49) Yan, J.; Gorai, P.; Ortiz, B.; Miller, S.; Barnett, S. A.; Mason, T.; Stevanović, V.; Toberer, E. S. Material descriptors for predicting thermoelectric performance. *Energy Environ. Sci.* **2015**, *8*, 983−994.
(50) Toberer, E. S.; Zevalkink, A.; Snyder, G. J. Phonon engineering through crystal chemistry. *J. Mater. Chem.* **2011**, *21*, 15843−15852.
(51) Francisco, E.; Recio, J. M.; Blanco, M. A.; Pendás, A. M.; Costales, A. Quantum-mechanical study of thermodynamic and bonding properties of MgF_2. *J. Mater. Chem. A* **1998**, *102*, 1595−1601.

https://doi.org/10.1021/acsomega.1c02172
ACS Omega 2021, 6, 18269−18280